ACS OMEGA

http://pubs.acs.org/journal/acsodf

Article

Promising Rare-Earth-Doped, Electrospun, ZnO Nanofiber N-type Semiconductor for Betavoltaic Batteries

Meng Zhang, Weijun Zhao, Jingxin Wu, Zhanqiang Li, Liyan Xue, Fan Yang,* Fengzhi Tan,* and Heng Chen*

Cite This: *ACS Omega* 2023, 8, 17644−17652

Read Online

ACCESS | Metrics & More | Article Recommendations

ABSTRACT: Betavoltaic batteries, as a kind of ultimate battery, have attracted much attention. ZnO is a promising wide-bandgap semiconductor material that has great potential in solar cells, photodetectors, and photocatalysis. In this study, rare-earth (Ce, Sm, and Y)-doped ZnO nanofibers were synthesized using advanced electrospinning technology. The structure and properties of the synthesized materials were tested and analyzed. As betavoltaic battery energy conversion materials, the results show that rare-earth doping increases the UV absorbance and the specific surface area and slightly reduces the band gap. In terms of electrical performance, a deep UV (254 nm) and X-ray source (10 keV) were used to simulate a radioisotope β-source to evaluate the basic electrical properties. Among them, the output current density of Y-doped ZnO nanofibers can reach 87 nA·cm^{-2}, which is 78% higher than that of traditional ZnO nanofibers, by deep UV. Besides, the photocurrent response of Y-doped ZnO nanofibers is superior to that of Ce-doped and Sm-doped ZnO nanofibers by soft X-ray. This study provides a basis for rare-earth-doped ZnO nanofibers as energy conversion devices used in betavoltaic isotope batteries.

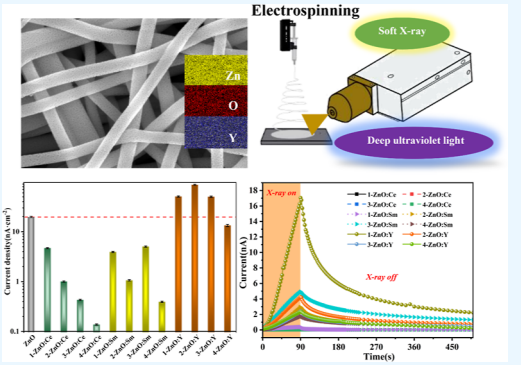

INTRODUCTION

With the proposal and development of fourth-generation advanced nuclear energy systems, radioisotope batteries, as an important branch of nuclear energy systems,[1,2] have attracted extensive attention owing to their high energy density, long lifetime, environmental stability, and miniaturization,[3−5] which are widely used in special fields, such as deep space, deep sea, polar, and medical devices. The economical and safe betavoltaic effect is a kind of energy transfer mode of radioisotope batteries. The principle is that β-particles interact with semiconductor materials to realize energy conversion.[6] Betavoltaic batteries are composed of β-source and a semiconductor energy conversion device. Since the 1970s, Olsen et al. proposed that wide-bandgap semiconductors have high energy conversion efficiency.[7] Researchers subsequently developed a series of wide band gap semiconductors: gallium nitride (GaN),[8] silicon carbide (SiC),[9] zinc oxide (ZnO),[10] titanium dioxide (TiO_2), and diamond.[11] Among wide-bandgap semiconductors of wide interest, ZnO has attracted particular attention because of high radiation tolerance, excellent chemical stability, low cost, and environmental friendliness.[12,13] Moreover, ZnO exhibits a high exciton binding energy (60 meV), a high breakdown strength, and much higher electron mobility than titanium oxide (TiO_2) (155 cm^2·V^{-1}·s^{-1} vs 10^{-5} cm^2·V^{-1}·s^{-1}), which would be favorable for electron transmission.[14,15] Among the many forms of ZnO, one-dimensional (1-D) ZnO nanofibers with the surface effect and the quantum-size effect have a large specific surface area and 1-D charge transport.[16] Therefore, 1-D ZnO nanofibers will have enormous potential in betavoltaic batteries.

Rare-earth (RE) elements, including the 15 lanthanides (La−Lu) and 2 group IIIB elements (Sc and Y), have a special 4f-5d electron ground state.[17] RE elements have a large atomic radius and a weak binding ability of the nucleus for the outer layer of electrons, so the electrons can transition between multiple energy levels and have strong chemical activity.[18,19] Doping RE elements into ZnO nanofibers is a promising method for material modification.[20−22] Doping nanomaterials with RE ions can adjust the crystal phase, conductivity, bandgap, and electronic configuration of the nanomaterials to endow them with rich optical, electrical, magnetic, and catalytic properties.[23−25] For instance, Ji et al. reported incorporation of RE ions (Tb, Dy, and Er) into ZnO nanostructures, observing dramatic splitting and enhancement

Received: January 3, 2023
Accepted: April 25, 2023
Published: May 8, 2023

of the intra-4f transition in photoluminescence excitation spectra.[26] Eu ions have been doped into ZnO nanostructured catalysts to enhance their photocatalytic activity toward organic pollutants by reducing the bandgap, trapping photo-induced electrons, and suppressing electron−hole recombination.[27] Tb ions have also been doped into ZnO nanorod bundles, exhibiting superparamagnetism at room temperature and ferromagnetism at 5 K.[28] However, there are few reports evaluating the application potential of RE-doped ZnO nanomaterials in nuclear power conversion.

New developments in electrospinning include nanofiber ceramic semiconductors.[29] Electrospun ceramic fibers offer properties that are difficult to achieve in other nanostructures, viz., (i) large aspect ratio and nanofiber volume make ion doping easier, (ii) accurate control of their thickness, size, and shape, and (iii) heat treatment can improve crystallinity without reducing nanofiber surface area.[30−33] The preparation of semiconductor ceramic nanofibers by electrospinning has been widely used in third-generation solar cells, electricity and photocatalysis systems, energy storage devices, and other fields.[34,35]

Due to the demand for semiconductor materials for energy conversion based on betavoltaic batteries, a series of RE-doped ZnO nanofibers were prepared by an electrospinning process and an RE modification method, doping light RE elements (Ce), medium RE elements (Sm), or heavy RE elements (Y). The potential application of the RE-doped nanofibers was evaluated with deep ultraviolet (UV) and soft X-ray instead of a β-source. This study will provide a good reference for the preparation of betavoltaic effect conversion devices in the future.

EXPERIMENTAL SECTION

Preparation of ZnO/Ce, ZnO/Sm, and ZnO/Y Nanofibers. In a typical experiment, different molar ratios of zinc acetate and cerium nitrate hexahydrate, samarium (III) nitrate hexahydrate, or yttrium nitrate hexahydrate were dissolved in a 7:3 v/v of *N*,*N*-dimethylformamide and acetylacetone solvent under magnetic stirring to dissolve them. Then, an appropriate amount of polyvinylpyrrolidone (PVP) was dissolved in the above solution under magnetic stirring to obtain a homogeneous precursor solution. The prepared electrospinning solution was carefully sucked into a 10 mL syringe, which was horizontally fixed by electrospinning equipment. A voltage of 23 kV was applied between the needle and the collection plate at a distance of 15 cm. The feeding rate was constant at 1.2 mL·h^{-1}. The electrospinning deposition was conducted in air (temperature: 24 °C, humidity: 35%). The obtained nanofibers were calcined at 500 °C for 1 h (heating rate: 1 °C/min) using a programmable furnace after drying at 80 °C for 12 h to obtain pure ZnO nanofibers and RE-doped ZnO nanofibers. The specific experimental process is shown in Scheme 1.

Material Characterization and Simulated β-Radioactive Source Measurement. The crystal structures of the samples were characterized using X-ray powder diffraction (XRD, Mini flex 600). The microstructure morphologies of the samples were characterized using field emission scanning electron microscopy (SEM, Apreo S LoVac). High-resolution images of single nanofibers were obtained using high-resolution transmission electron microscopy (TEM, FEI/Talos F200X G2). The elemental information of the samples was characterized using X-ray photoelectron spectroscopy (XPS, Thermo Fisher Scientific K-alpha$^+$). The ultraviolet−visible light (UV−Vis) absorption of the samples was characterized using a UV−Vis spectrophotometer (Agilent Cary 5000, USA).

Scheme 1. Schematic Diagram of the Preparation Process of the Nanofiber Ceramic

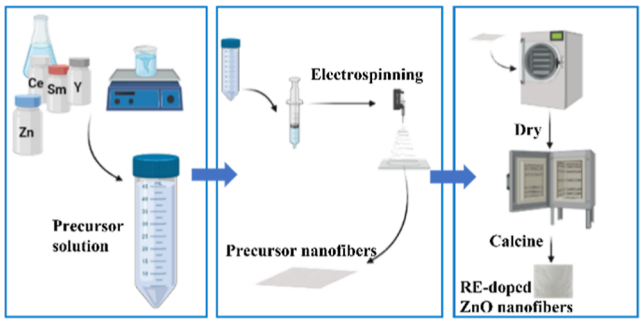

β-Source has great limitations, which makes it difficult for researchers to test and verify materials in the radiation at the beginning of the experiment. It is generally tested by radiation simulation. For example, Li et al. used lasers to simulate radiation effects because laser irradiation of semiconductor devices can produce electrical characteristics similar to some radiation effects.[36] Kim et al. reported the electrical performance of a manufactured betavoltaic cell evaluated by electron-beam irradiation.[37] Here, an UV light source system (CEL-LPH120-254) with 254 nm and a MagPro X-ray source (TUB00146-W06, Japan) with 10 keV are used to simulate β-source. The output currents of the samples were characterized using a picoammeter (Keithley 6485, USA). All measurements were performed in a dark shielding box at room temperature (298 K).

RESULTS AND DISCUSSION

Figure 1a depicts a physical image of the precursor of zinc oxide nanofibers. The thickness and size of the precursor can be controlled, making it a versatile material that can be applied in various fields. From the SEM image shown in Figure 1b, it can be observed that the surface of the precursor nanofibers is smooth, the length is continuous, and the diameter is approximately 200 nm. The ZnO nanofibers after being calcined at 500 °C are shown in Figure 1c. Through the decomposition of PVP and dissolution, as well as the formation of ZnO, the surface of the fibers becomes rough, but they still maintain a continuous state. The diameter of the fibers decreases to about 100 nm. Figure 1d−f displays SEM images of calcined Ce-doped, Sm-doped, and Y-doped ZnO nanofibers. Apparently, the diameter of the nanofibers increases to around 300 nm due to the addition of rare-earth ions. This is because the addition of rare-earth ions leads to an increase in the conductivity of the precursor solution, which in turn strengthens the electric field force during electrospinning, leading to a relative weakening of fiber stretching. The Ce-doped and Sm-doped ZnO nanofibers have raised grains on their surfaces, while the surface of the Y-doped ZnO nanofibers is relatively flat. A TEM image of a single nanofiber is shown in Figure 1g, which shows continuous grain nanofibers. A lattice image is shown in Figure 1h, indicating that the ZnO single grains are highly crystalline. The lattice spacing along the (002) direction

https://doi.org/10.1021/acsomega.3c00039
ACS Omega 2023, 8, 17644−17652

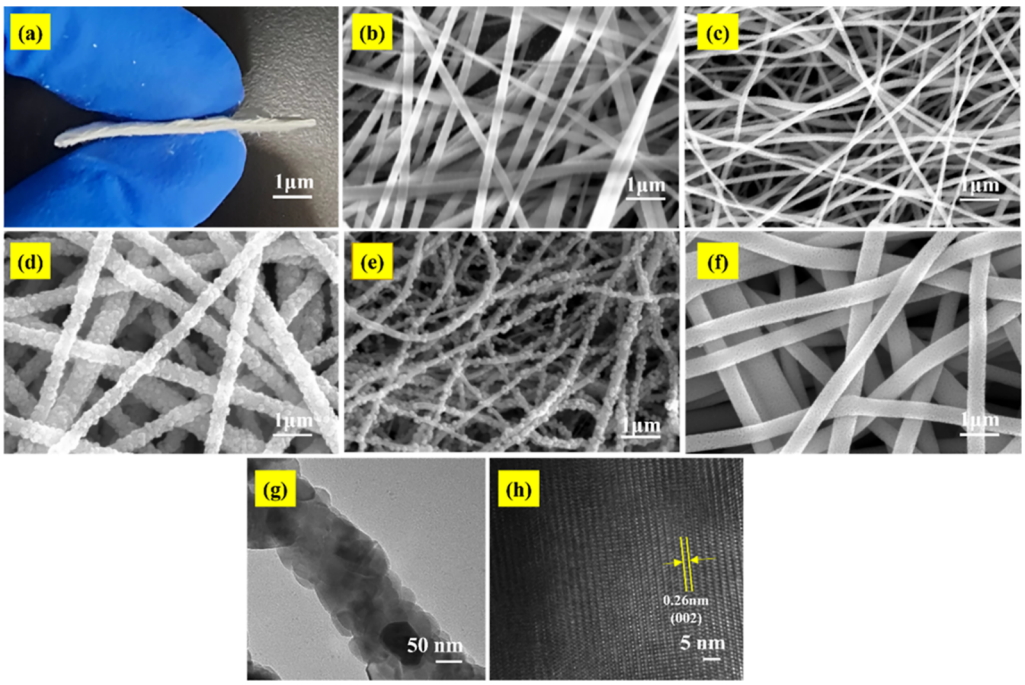

Figure 1. (a) Macroscopic side view and top view of a nanofiber sample. SEM images of (b) ZnO nanofibers before calcination, (c) ZnO nanofibers, (d) Ce-doped ZnO nanofibers, (e) Sm-doped ZnO nanofibers, and (f) Y-doped ZnO nanofibers. (g) Low- and (h) high-magnification TEM images of a single ZnO nanofiber.

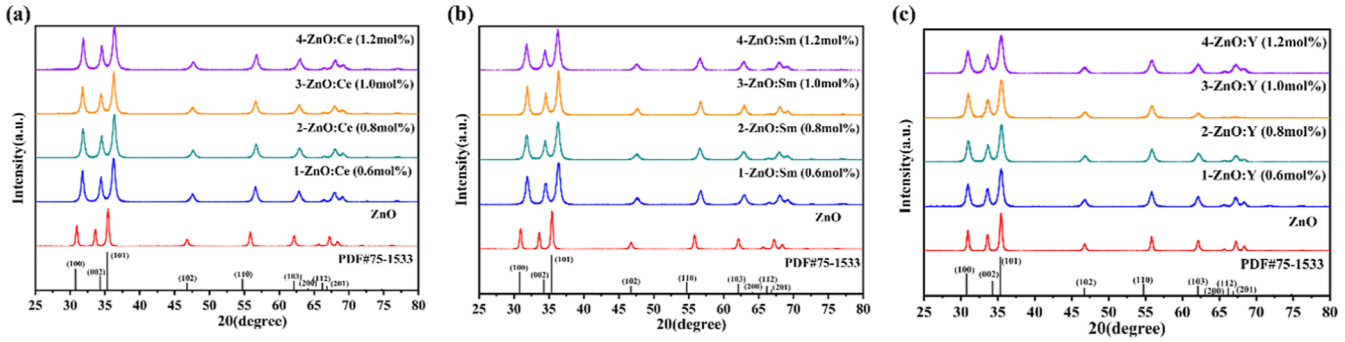

Figure 2. XRD patterns of (a) Ce-doped ZnO nanofibers, (b) Sm-doped ZnO nanofibers, and (c) Y-doped ZnO nanofibers.

indicated by yellow lines is 0.26 nm, which is consistent with the wurtzite crystal structure of ZnO.

Figure 2a–c shows the XRD patterns of the Ce-doped, Sm-doped, and Y-doped ZnO nanofibers compared to those of the pure ZnO nanofibers. From the XRD pattern, all samples show nine diffraction peaks of the ZnO nanofibers corresponding to the (100), (002), (101), (102), (110), (103), (200), (112), and (201) planes of the wurtzite crystal structure at 30.98, 33.63, 35.44, 46.78, 55.86, 62.16, 65.66, 67.26, and 68.46°, respectively.[38] All diffraction peaks consistent with the reported data confirm that ZnO has a wurtzite hexagonal phase. No characteristic peaks of other RE oxides or other impurities are observed.

After doping, the morphology of the ZnO nanofibers changes, which affects the specific surface area and porosity of the ZnO nanofibers. The N_2 adsorption–desorption isotherms of pure ZnO nanofibers and RE-doped ZnO nanofibers are shown in Figure 3a–d. All ZnO samples show IV-type isotherms with an H3-type hysteresis loop,[39] which indicates that the nanofibers maintain a mesoporous structure. The pore size distribution curves of the corresponding samples were also obtained by using the Barrett–Joyner–Halenda (BJH) calculation method, and the results are shown in Figure 3e–h. As shown in Figure 3e, the specific surface area of the pure ZnO nanofibers is nearly 9.03 $m^2 \cdot g^{-1}$, and its pore volume is 0.06 $cm^3 \cdot g^{-1}$. As shown in Figure 3f–h, the doping with RE ions increases the specific surface area of the ZnO nanofibers.

To further investigate the elemental compositions of the Ce-doped and Sm-doped ZnO nanofibers and their chemical bonding states, XPS tests were conducted. The measured scanned peaks in Figure 4a, c could be identified as corresponding to C, O, Zn, Ce, and Sm elements, verifying the presence of these elements in the Ce-doped and Sm-doped ZnO nanofibers. All data were corrected by referencing them to the C 1s peak (set at 284.8 eV) before processing the spectroscopic data. After Gaussian fitting of the curves, Zn 2p peaks (Figure 4b) appear at two positions of 1021.4 and 1044.45 eV, corresponding to Zn $2p_{3/2}$ and Zn $2p_{1/2}$, respectively.[40] The Zn 2p peaks of the Ce-doped ZnO nanofiber materials are slightly shifted to lower binding energies compared to the standard spectrum of the ZnO

https://doi.org/10.1021/acsomega.3c00039
ACS Omega 2023, 8, 17644–17652

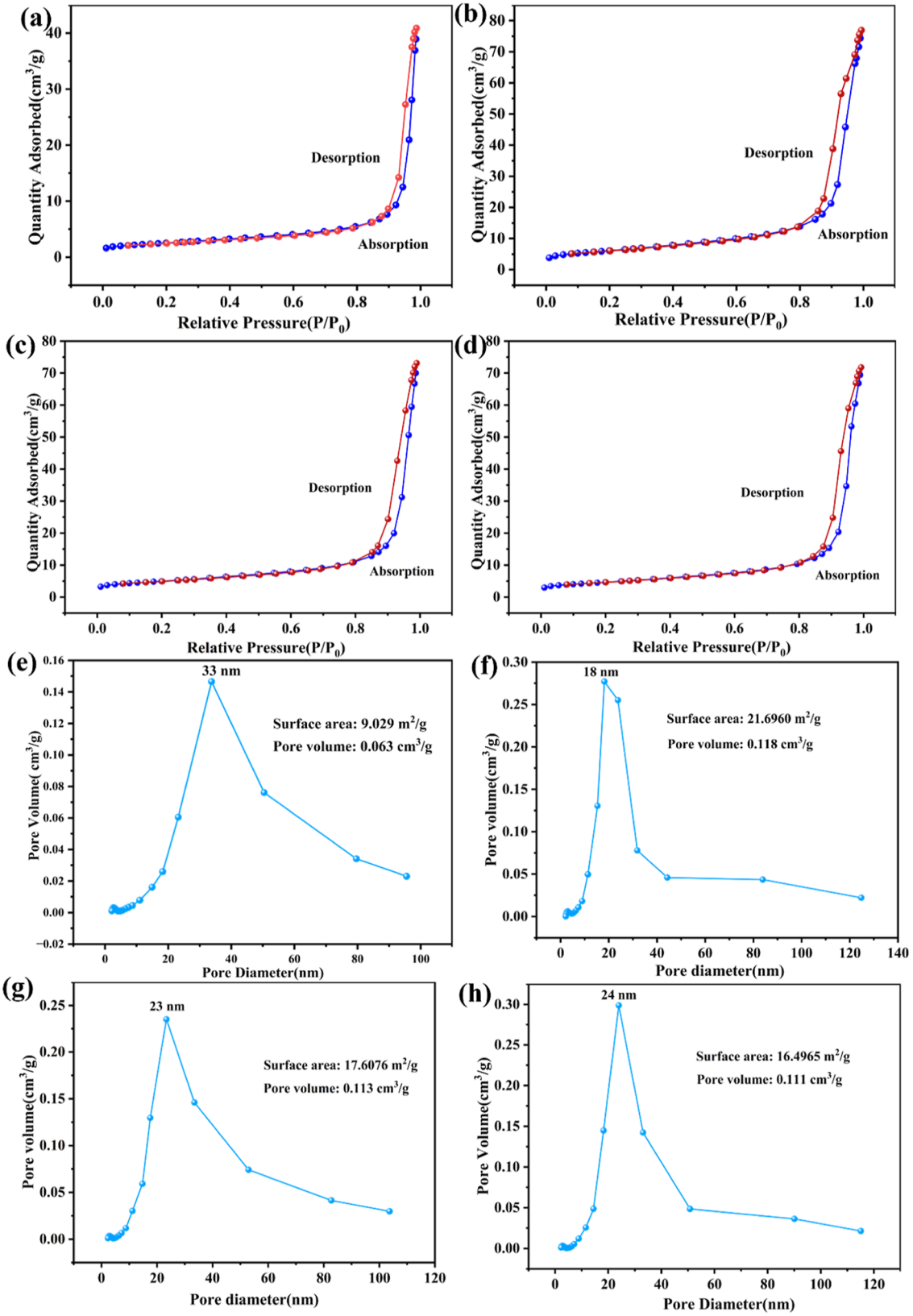

Figure 3. N_2 adsorption−desorption isotherms of (a) ZnO nanofibers, (b) Ce-doped ZnO nanofibers, (c) Sm-doped ZnO nanofibers, and (d) Y-doped ZnO nanofibers; pore distributions of (e) ZnO nanofibers, (f) Ce-doped ZnO nanofibers, (g) Sm-doped ZnO nanofibers, and (h) Y-doped ZnO nanofibers.

material. This is due to the shift of Ce electrons toward Zn, which corresponds to a relatively high electron density on Zn, and the corresponding ability of the Zn nucleus to bind external electrons will be weakened, resulting in a decrease in the binding energy. The successful doping of Ce atoms into the ZnO crystal is proven. In addition, by fitting, the Ce 3d

https://doi.org/10.1021/acsomega.3c00039
ACS Omega 2023, 8, 17644−17652

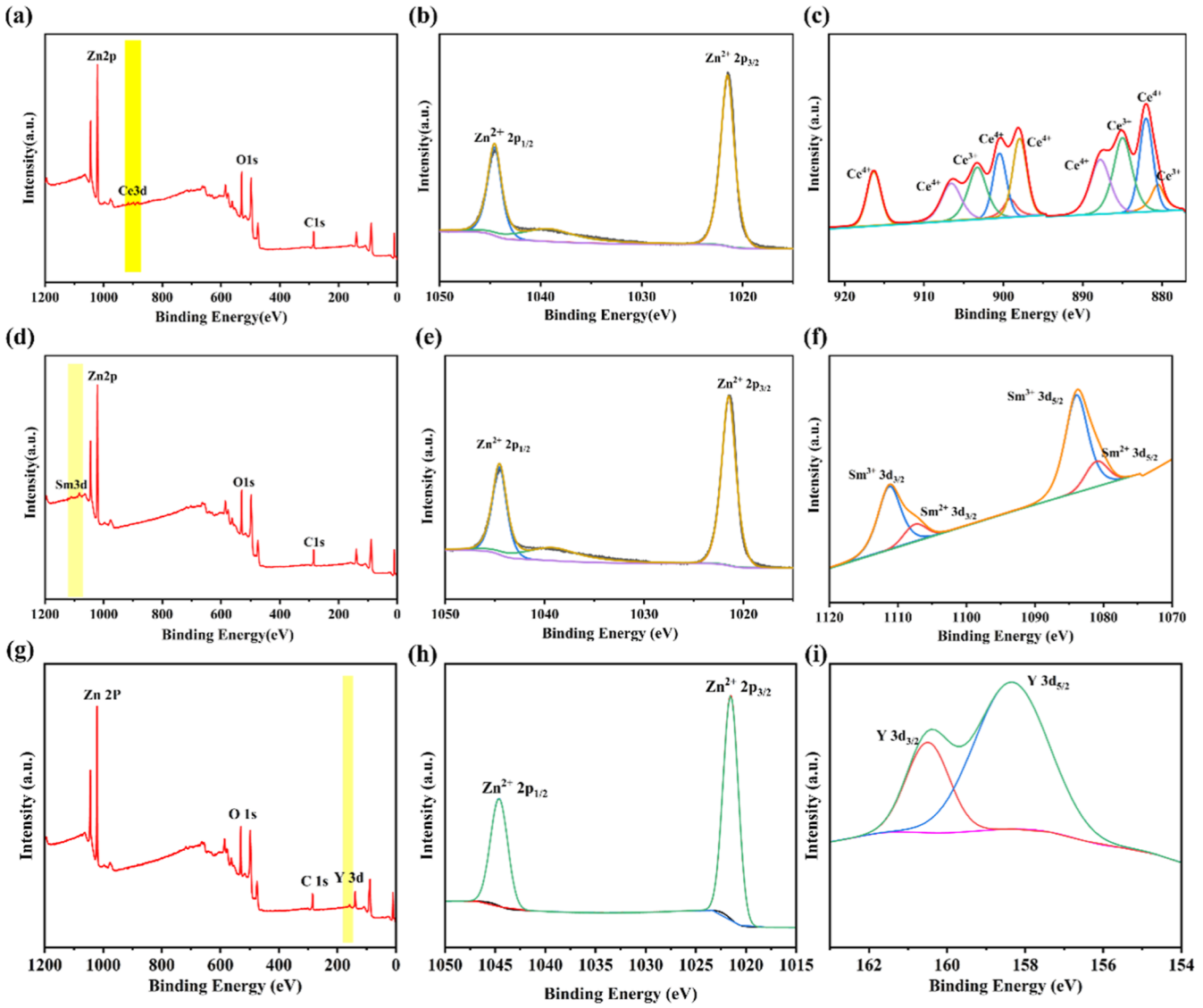

Figure 4. XPS spectra of (a) the full survey scan, (b) Zn 2p, and (c) Ce 3d for the Ce-doped ZnO nanofiber material. XPS spectra of (d) the full survey scan, (e) Zn 2p, and (f) Sm 3d for the Sm-doped ZnO nanofiber material. XPS spectra of (g) the full survey scan, (h) Zn 2p, and (i) Y 3d for the Y-doped ZnO nanofiber material.

spectrum (Figure 4c) of the Ce-doped ZnO nanofiber material was divided into 9 peaks. The three peaks located at 880.5, 884.8, and 903.3 eV are attributed to the Ce(III) atom. The six peaks located at 881.9, 887.7, 897.8, 900.5, 906.5, and 916.5 eV are attributed to the Ce(IV) atom.[41−43] This indicates that the Ce element in the material simultaneously exists in two different oxidation states. Figure 4e shows the Zn 2p peaks of the Sm-doped ZnO nanofiber materials. The results are similar to those of the Ce-doped sample. In the Sm 3d spectrum (Figure 4d), the four peaks belong to Sm $3d_{3/2}$ and Sm $3d_{5/2}$. The binding energies of 1080.8, 1083.8, 1107.3, and 1111.1 eV indicate the existence of Sm^{2+} and Sm^{3+}, which agree with the literature data. Figure 4g displays the full-spectrum XPS spectrum of ZnO/Y, which indicates the presence of Zn, Y, and O elements. In addition, the valence states of Zn and Y elements were investigated. As shown in Figure 4h, the Zn 2p spectrum exhibits two main spin−orbit splitting components, namely $2p_{3/2}$ and $2p_{1/2}$, with binding energies of 1021 and 2044 eV, respectively. These results are consistent with the literature and indicate that the obtained Zn has a +2 ionic state. Figure 4i shows the high-resolution spectrum of the Y element, which includes two spin−orbit dipole components, namely Y $3d_{5/2}$ and Y $3d_{3/2}$, with binding energies of 158.4 and 160.4 eV, respectively. These two doublets are attributed to the Y−O bond length,[44,45] confirming the presence of Y^{3+} ions in the Y-doped ZnO nanofibers.

The effects of Ce, Sm, and Y doping ZnO on UV absorption were investigated, as shown in Figure 5. From Figure 5a, with increasing Ce doping content, the UV absorbance of the sample gradually increases and tends to stabilize. Compared with the pure ZnO sample, the UV absorbance of 4-ZnO/Ce is most obviously enhanced, increasing by 20%. From Figure 5c, with increasing Sm doping content, the UV absorbance of the sample first increases and then decreases. Compared with the pure ZnO sample, the absorbance of both 1-ZnO/Sm and 3-ZnO/Sm increases by 10%. From Figure 5e, with increasing Y doping content, the UV absorbance of the sample first increases and then decreases. Compared with the pure ZnO sample, the UV

https://doi.org/10.1021/acsomega.3c00039
ACS Omega 2023, 8, 17644−17652

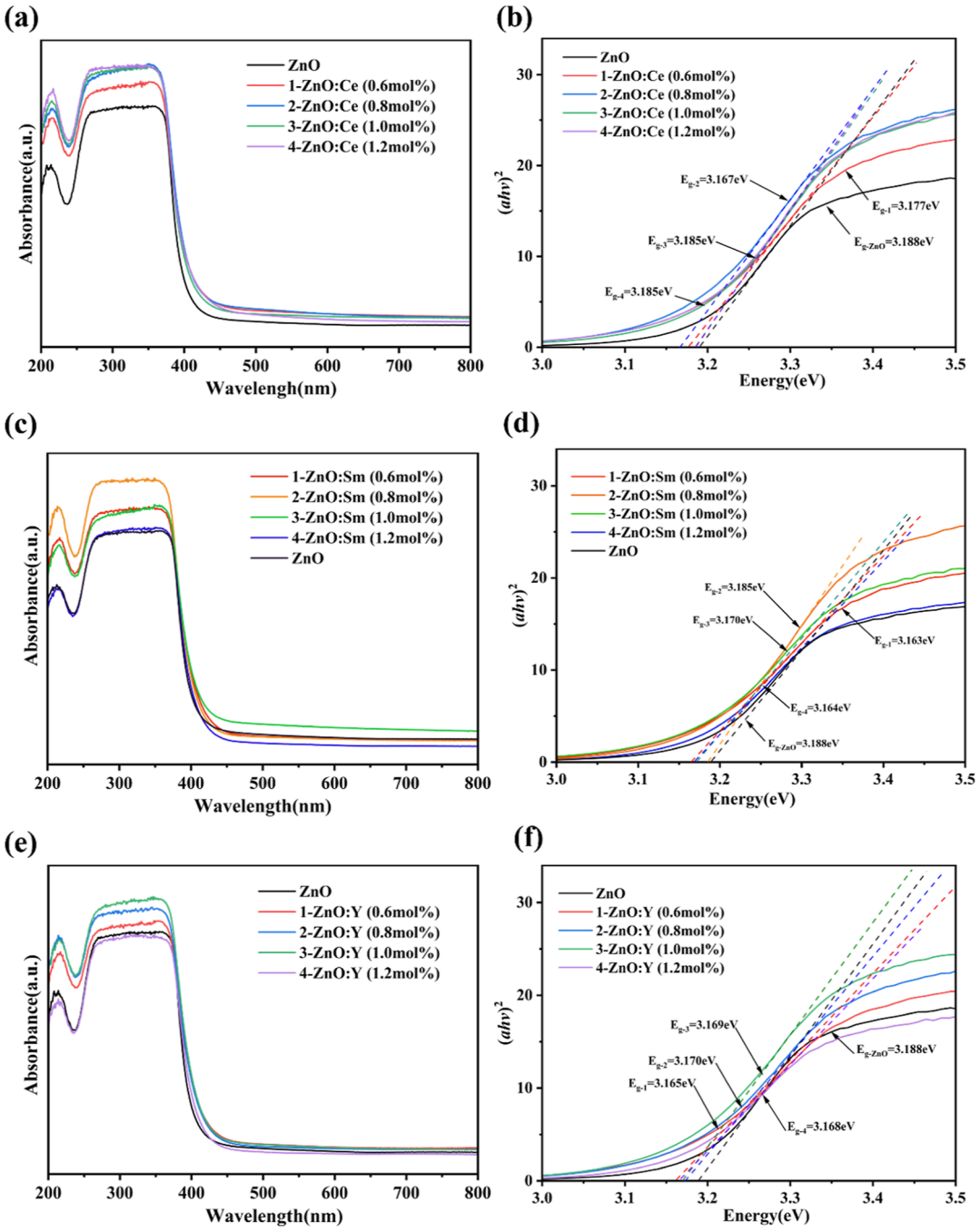

Figure 5. (a) UV−Vis absorption spectra and (b) calculated bandgaps of Ce-doped ZnO nanofibers; (c) UV−Vis absorption spectra and (d) calculated bandgaps of Sm-doped ZnO nanofibers; (e) UV−Vis absorption spectra and (f) calculated bandgaps of Y-doped ZnO nanofibers.

absorbance of 4-ZnO/Y decreases by 3%. The bandgaps of all samples were calculated from the main absorption edge of the spectra in Figure 5b,d,f.[46] The bandgap of pure ZnO nanofibers is 3.18 eV. Compared with pure ZnO nanofibers, the bandgaps of the RE-doped ZnO nanofibers are slightly smaller, which can be attributed to the defects caused by doping.

To evaluate the RE-doped ZnO nanofiber materials in a cost-effective manner, deep UV and X-rays were used to qualitatively simulate the beta-electrochemical performance. Without an external voltage bias, the samples can generate a photocurrent under UV radiation. Figure 6 shows the largest output current densities of Ce-doped, Sm-doped, Y-doped, and pure ZnO nanofiber samples after ∼1800 s of deep UV irradiation. 2-ZnO/Y shows a maximum output current density of 87 nA·cm^{-2}. 4-ZnO/Y shows a lower output current than the pure ZnO nanofibers, which can be attributed to its lower UV absorbance than that of the pure ZnO nanofibers. The output current of the materials is related not only to the UV absorbance but also to the morphology and structure. The output currents of both the Ce-doped and Sm-doped ZnO nanofiber materials are lower than those of the Y-doped ZnO nanofiber materials. This may be due to the fact the the Y ion has a stable electronic structure, which makes Y ions more stable in the crystal, improves the efficiency of electron transfer, and prolongs electron lifetime.[21]

https://doi.org/10.1021/acsomega.3c00039
ACS Omega 2023, 8, 17644−17652

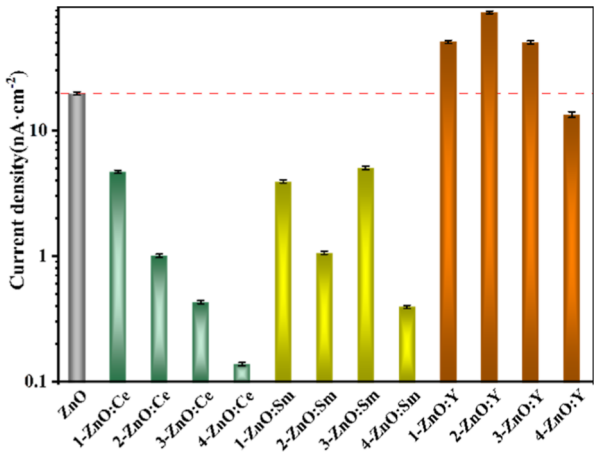

Figure 6. Largest output current densities of RE-doped ZnO nanofiber materials under 14 mW·cm^{-2} UV irradiation for 1800 s.

On the other hand, Ce ions and Sm ions, due to their variable valence states, may cause a decrease in material performance and instability. In conclusion, the Y-doped ZnO nanofiber materials exhibit better photoelectric conversion efficiency.

To investigate the time-dependent photoresponses during the rise and fall phases, 90 s I−t tests of doped samples were performed. Figure 7a exhibits an actual photo of the samples under test and a sketch map. As shown in Figure 7b, 1-ZnO/Y enables the best photocurrent response compared with the other samples.

CONCLUSIONS

In this study, RE-doped (Ce, Sm, and Y) one-dimensional ZnO nanofibers were successfully prepared by a simple and cost-effective electrospinning technique and applied to battery energy conversion devices. The as-synthesized RE-doped ZnO nanofibers have a uniform surface morphology. According to SEM, the quality of the Y-doped ZnO nanofibers has improved. Compared with pure ZnO nanofibers, the specific surface area and UV absorbance of Y-doped ZnO nanofibers are increased by 82 and 10%, respectively. A deep UV light source and soft X-ray were used to simulate a β-source to evaluate the basic electrical properties of the materials. The results indicate that the output current density and photocurrent response for heavy RE (Y) doping are superior to those for light RE (Ce) doping and medium RE (Sm) doping. The maximum output current density of 2-ZnO/Y reaches 87 nA·cm^{-2}. 1-ZnO/Y sample exhibits the best photocurrent response effect by soft X-ray. In a word, Y-doped ZnO nanofibers have greater application potential in betavoltaic battery energy conversion devices.

AUTHOR INFORMATION

Corresponding Authors

Fan Yang − *Fujian Province Joint Innovation Key Laboratory of Fuel and Materials in Clean Nuclear Energy System, Fujian Institute of Research on the Structure of Matter, Chinese Academy of Sciences, 350002 Fuzhou, China; Fujian Science & Technology Innovation Laboratory for Optoelectronic Information of China, 350108 Fuzhou, China; Xiamen Institute of Rare Earth Materials, Haixi Institute and Xiamen Key Laboratory of Rare Earth Photoelectric Functional Materials, Xiamen Institute of Rare Earth Materials, Haixi Institute, Chinese Academy of Sciences, 361021 Xiamen, China;* orcid.org/0000-0002-5972-5466; Email: fanyang2013@fjirsm.ac.cn

Fengzhi Tan − *School of Light Industry and Chemical Engineering, Dalian Polytechnic University, 116034 Dalian, China*; Email: tanfz@dlpu.edu.cn

Heng Chen − *Fujian Province Joint Innovation Key Laboratory of Fuel and Materials in Clean Nuclear Energy System, Fujian Institute of Research on the Structure of Matter, Chinese Academy of Sciences, 350002 Fuzhou, China; Fujian Science & Technology Innovation Laboratory for Optoelectronic Information of China, 350108 Fuzhou, China; Xiamen Institute of Rare Earth Materials, Haixi Institute and Xiamen Key Laboratory of Rare Earth Photoelectric Functional Materials, Xiamen Institute of Rare Earth Materials, Haixi Institute, Chinese Academy of Sciences, 361021 Xiamen, China*; Email: xmchenheng@fjirsm.ac.cn

Authors

Meng Zhang − *School of Light Industry and Chemical Engineering, Dalian Polytechnic University, 116034 Dalian, China; Fujian Province Joint Innovation Key Laboratory of Fuel and Materials in Clean Nuclear Energy System, Fujian*

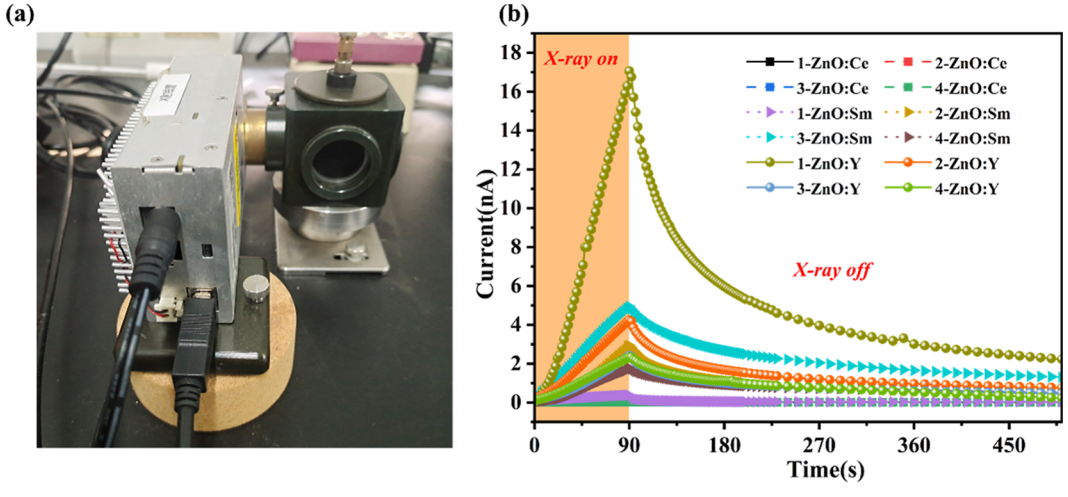

Figure 7. (a) Actual photo of samples in the soft X-ray test; (b) time-dependent photoresponses of the doped samples under soft X-rays.

https://doi.org/10.1021/acsomega.3c00039
ACS Omega 2023, 8, 17644−17652

Institute of Research on the Structure of Matter, Chinese Academy of Sciences, 350002 Fuzhou, China; Fujian Science & Technology Innovation Laboratory for Optoelectronic Information of China, 350108 Fuzhou, China; Xiamen Institute of Rare Earth Materials, Haixi Institute and Xiamen Key Laboratory of Rare Earth Photoelectric Functional Materials, Xiamen Institute of Rare Earth Materials, Haixi Institute, Chinese Academy of Sciences, 361021 Xiamen, China

Weijun Zhao − *Fujian Province Joint Innovation Key Laboratory of Fuel and Materials in Clean Nuclear Energy System, Fujian Institute of Research on the Structure of Matter, Chinese Academy of Sciences, 350002 Fuzhou, China; Fujian Science & Technology Innovation Laboratory for Optoelectronic Information of China, 350108 Fuzhou, China; Xiamen Institute of Rare Earth Materials, Haixi Institute and Xiamen Key Laboratory of Rare Earth Photoelectric Functional Materials, Xiamen Institute of Rare Earth Materials, Haixi Institute, Chinese Academy of Sciences, 361021 Xiamen, China*

Jingxin Wu − *Fujian Province Joint Innovation Key Laboratory of Fuel and Materials in Clean Nuclear Energy System, Fujian Institute of Research on the Structure of Matter, Chinese Academy of Sciences, 350002 Fuzhou, China; Fujian Science & Technology Innovation Laboratory for Optoelectronic Information of China, 350108 Fuzhou, China; Xiamen Institute of Rare Earth Materials, Haixi Institute and Xiamen Key Laboratory of Rare Earth Photoelectric Functional Materials, Xiamen Institute of Rare Earth Materials, Haixi Institute, Chinese Academy of Sciences, 361021 Xiamen, China*

Zhanqiang Li − *Fujian Province Joint Innovation Key Laboratory of Fuel and Materials in Clean Nuclear Energy System, Fujian Institute of Research on the Structure of Matter, Chinese Academy of Sciences, 350002 Fuzhou, China; Fujian Science & Technology Innovation Laboratory for Optoelectronic Information of China, 350108 Fuzhou, China; Xiamen Institute of Rare Earth Materials, Haixi Institute and Xiamen Key Laboratory of Rare Earth Photoelectric Functional Materials, Xiamen Institute of Rare Earth Materials, Haixi Institute, Chinese Academy of Sciences, 361021 Xiamen, China*

Liyan Xue − *Fujian Province Joint Innovation Key Laboratory of Fuel and Materials in Clean Nuclear Energy System, Fujian Institute of Research on the Structure of Matter, Chinese Academy of Sciences, 350002 Fuzhou, China; Fujian Science & Technology Innovation Laboratory for Optoelectronic Information of China, 350108 Fuzhou, China; Xiamen Institute of Rare Earth Materials, Haixi Institute and Xiamen Key Laboratory of Rare Earth Photoelectric Functional Materials, Xiamen Institute of Rare Earth Materials, Haixi Institute, Chinese Academy of Sciences, 361021 Xiamen, China*

Complete contact information is available at: https://pubs.acs.org/10.1021/acsomega.3c00039

Notes

The authors declare no competing financial interest.

■ ACKNOWLEDGMENTS

This work was supported financially by the National Key Research and Development Program of China (no.2019YFC0605000), the National Key Research and Development Program of China (no.2022YFB3504302), the independent deployment project of the Fujian Science & Technology Innovation Laboratory for Optoelectronic Information of China (no.2021ZZ109), the Ganjiang Innovation Research Institute of the Chinese Academy of Sciences (E055A002), the Lingchuang Research Project of the China National Nuclear Corporation, the Fujian Provincial Natural Fund Project [grant no. 2021J05101], and the CAST Young Talent Support Project.

■ REFERENCES

(1) Mincher, B. J. The Nuclear Renaissance: Producing Environmentally Sustainable Nuclear Power. *ACS Symp. Ser.* **2010**, *1046*, 3−10.

(2) Li, G.; Zhang, S.; Zhou, Y. A review of radioisotope batteries. *Chin. Sci. Bull.* **2017**, *62*, 1831−1845.

(3) Li, G.; Zhao, C.; Liu, Y.; Ren, J.; Zhang, Z.; Di, H.; Jiang, W.; Mei, J.; Zhao, Y. High-Performance Perovskite Betavoltaics Employing High-Crystallinity $MAPbBr_3$ Films. *ACS Omega* **2021**, *6*, 20015−20025.

(4) Wang, N.; Zheng, R.; Chi, T.; Jiang, T.; Ding, Z.; Li, X.; Liu, S.; Zhang, L.; San, H. Betavoltaic-powered electrochemical cells using TiO2 nanotube arrays incorporated with carbon nanotubes. *Compos. B Eng.* **2022**, *239*, 109952 Elsevier Ltd.

(5) Chen, C.; Wang, N.; Zhou, P.; San, H.; Wang, K.; Chen, X. Electrochemically reduced graphene oxide on well-aligned titanium dioxide nanotube arrays for betavoltaic enhancement. *ACS Appl. Mater. Interfaces* **2016**, *8*, 24638−24644.

(6) Song, Z.; Zhao, C.; Liao, F.; Zhao, Y. Perovskite-Betavoltaic Cells: A Novel Application of Organic−Inorganic Hybrid Halide Perovskites. *ACS Appl. Mater. Interfaces* **2019**, *11*, 32969−32977.

(7) Olsen, L. C. Betavoltaic Energy Conversion. *Energy Convers.* **1973**, *13*, 117−127.

(8) Han, X.; Yu, J.; Li, Z.; Wang, X.; Hao, Z.; Luo, Y.; Sun, C.; Han, Y.; Xiong, B.; Wang, J.; Li, H.; Zhang, Y.; Duan, B.; Ning, J.; Wu, H.; Wang, L. Remote Epitaxy and Exfoliation of GaN via Graphene. *ACS Appl. Electron. Mater.* **2022**, *4*, 5326−5332.

(9) Tsai, A.; Aghajamali, A.; Dontschuk, N.; Johnson, B. C.; Usman, M.; Schenk, A. K.; Sear, M.; Pakes, C. I.; Hollenberg, L. C. L.; McCallum, J. C.; Rubanov, S.; Tadich, A.; Marks, N. A.; Stacey, A. Epitaxial Formation of SiC on (100) Diamond. *ACS Appl. Electron. Mater.* **2020**, *2*, 2003−2009.

(10) Chen, C.; Zhang, S.; Hu, B.; San, H.; Cheng, Z.; Hofmann, W. Non-aligned ZnO nanowires composited with reduced graphene oxide and single-walled carbon nanotubes for highly responsive UV−visible photodetectors. *Compos. B Eng.* **2019**, *164*, 640−647.

(11) Mandal, S.; Bautze, T.; Williams, O. A.; Naud, C.; Bustarret, E.; Omnes, F.; Rodiere, P.; Meunier, T.; Bauerle, C.; Saminadayar, L. The Diamond Superconducting Quantum Interference Device. *ACS Nano* **2011**, *5*, 7144−7148.

(12) Du, H.; Yang, W.; Yi, W.; Sun, Y.; Yu, N.; Wang, J. Oxygen-Plasma-Assisted Enhanced Acetone-Sensing Properties of ZnO Nanofibers by Electrospinning. *ACS Appl. Mater. Interfaces* **2020**, *12*, 23084−23093.

(13) Soonsen, S. M.; Lekshmi, B.; George, K. C. OPTICAL PROPERTIES OF ZnO NANOPARTICLES. *Acad. Rev.* **2009**, *1*, 57−68.

(14) Mali, S. S.; Kim, H.; Jang, W. Y.; Park, H. S.; Patil, P. S.; Hong, C. K. Novel Synthesis and Characterization of Mesoporous ZnO Nanofibers by Electrospinning Technique. *ACS Sustainable Chem. Eng.* **2013**, *1*, 1207−1213.

(15) Li, B.; Zeng, Z.; Qiao, J.; Yang, Y.; Xu, D.; Tian, H.; Liu, W.; Liu, J. Hollow ZnO/Fe3O4@C Nanofibers for Efficient Electromagnetic Wave Absorption. *ACS Appl. Nano Mater.* **2022**, *5*, 11617−11626.

(16) Chen, C.; Hu, B.; Wang, Z.; Lv, X.; Zhang, C.; Chen, B.; San, H.; Hofmann, W. Face-to-face intercrossed ZnO nanorod arrays with

https://doi.org/10.1021/acsomega.3c00039
ACS Omega 2023, 8, 17644−17652

extensive NR-NR homojunctions for a highly sensitive and self-powered ultraviolet photodetector. *Nano Energy* **2019**, *65*, 104042.
(17) Zheng, B.; Fan, J.; Chen, B.; Qin, X.; Wang, J.; Wang, F.; Deng, R.; Liu, X. Rare-Earth Doping in Nanostructured Inorganic Materials. *Chem. Rev.* **2022**, *122*, 5519−5603.
(18) Zeng, X.; Yuan, J.; Zhang, L. Synthesis and Photoluminescent Properties of Rare Earth Doped ZnO Hierarchical Microspheres. *J. Phys. Chem. C* **2008**, *112*, 3503−3508.
(19) Samarasekere, P.; Wang, X.; Kaveevivitchai, W.; Jacobson, A. J. Reactions of Rare Earth Hydrated Nitrates and Oxides with Formamide: Relevant to Recycling Rare Earth Metals. *Cryst. Growth Des.* **2015**, *15*, 1119−1128.
(20) Li, G.; Lu, X.; Zhao, W.; Su, C.; Tong, Y. Controllable Electrochemical Synthesis of Ce^{4+}-Doped ZnO Nanostructures from Nanotubes to Nanorods and Nanocages. *Cryst. Growth Des.* **2008**, *8*, 1276−1281.
(21) Commandeur, D.; Brown, G.; McNulty, P.; Dadswell, C.; Spencer, J.; Chen, Q. Yttrium-Doped ZnO Nanorod Arrays for Increased Charge Mobility and Carrier Density for Enhanced Solar Water Splitting. *J. Phys. Chem. C* **2019**, *123*, 18187−18197.
(22) Goodall, J. B. M.; Illsley, D.; Lines, R.; Makwana, N. M.; Darr, J. A. Structure−Property−Composition Relationships in Doped Zinc Oxides: Enhanced Photocatalytic Activity with Rare Earth Dopants. *ACS Comb. Sci.* **2015**, *17*, 100−112.
(23) Hossain, M. K.; Hossain, S.; Ahmed, M. H.; Khan, M. I.; Haque, N.; Raihan, G. A. A Review on Optical Applications, Prospects, and Challenges of Rare-Earth Oxides. *ACS Appl. Electron. Mater.* **2021**, *3*, 3715−3746.
(24) Kumar, V.; Ntwaeaborwa, O. M.; Soga, T.; Dutta, V.; Swart, H. C. Rare Earth Doped Zinc Oxide Nanophosphor Powder: A Future Material for Solid State Lighting and Solar Cells. *ACS Photonics* **2017**, *4*, 2613−2637.
(25) Isacfranklin, M.; Princy, L. E. M.; Rathinam, Y.; Kungumadevi, L.; Ravi, G.; Al-Sehemi, A. G.; Velauthapillai, D. Rare Earth-Doped MoS2for Supercapacitor Application. *Energy Fuels* **2022**, *36*, 6476−6482.
(26) Ji, S.; Yin, L.; Liu, G.; Zhang, L.; Ye, C. Synthesis of Rare Earth Ions-Doped ZnO Nanostructures with Efficient Host−Guest Energy Transfer. *J. Phys. Chem. C* **2009**, *113*, 16439−16444.
(27) Trandafilović, L. V.; Jovanović, D. J.; Zhang, X.; Ptasińska, S.; Dramićanin, M. D. Enhanced photocatalytic degradation of methylene blue and methyl orange by ZnO:Eu nanoparticles. *Appl. Catal., B* **2017**, *203*, 740−752.
(28) Li, G.; Lu, X.; Su, C.; Tong, Y. Facile Synthesis of Hierarchical ZnO:Tb^{3+} Nanorod Bundles and Their Optical and Magnetic Properties. *J. Phys. Chem. C* **2008**, *112*, 2927−2933.
(29) Wang, S.; Shao, H.; Liu, Y.; Tang, C.; Zhao, X.; Ke, K.; Bao, R.; Yang, M.; Yang, W. Boosting piezoelectric response of PVDF-TrFE via MXene for self-powered linear pressure sensor. *Compos. Sci. Technol.* **2021**, *202*, 108600.
(30) Reddy, M. V.; Jose, R.; Teng, T. H.; Chowdari, B. V. R.; Ramakrishna, S. Preparation and electrochemical studies of electrospun TiO2nanofibersand molten salt method nanoparticles. *Electrochim. Acta* **2010**, *55*, 3109−3117.
(31) Viet, A. L.; Reddy, M. V.; Jose, R.; Chowdari, B. V. R.; Ramakrishna, S. Nanostructured Nb_2O_5 Polymorphs by Electrospinning for Rechargeable Lithium Batteries. *J. Phys. Chem. C* **2010**, *114*, 664−671.
(32) Reddy, M. V.; Jose, R.; Viet, A. L.; Ozoemena, K. I.; Chowdari, B. V. R.; Ramakrishna, S. Studies on the lithiumion diffusion coefficients of electrospun Nb_2O_5 nanostructures using galvanostatic intermittent titration and electrochemical impedance spectroscopy. *Electrochim. Acta* **2014**, *128*, 198−202.
(33) Yue, L.; Zhao, H.; Wu, Z.; Liang, J.; Lu, S.; Chen, G.; Gao, S.; Zhong, B.; Guo, X.; Sun, X. Recent advances in electrospun one-dimensional carbon nanofiber structures/heterostructures as anode materials for sodium ion batteries. *J. Mater. Chem. A.* **2020**, *8*, 11493−11510.
(34) Liang, J.; Zhao, H.; Yue, L.; Fan, G.; Li, T.; Lu, S.; Chen, G.; Gao, S.; Asiri, A. M.; Sun, X. Recent advances in electrospun nanofibers for supercapacitors. *J. Mater. Chem. A.* **2020**, *8*, 16747−16789.
(35) Zhao, W.; Yang, F.; Liu, Z.; Chen, H.; Shao, Z.; Zhang, X.; Wang, K.; Xue, L. A novel (La0.2Sm0.2Eu0.2Gd0.2Tm0.2)2Zr2O7 high-entropy ceramic nanofiber with excellent thermal stability. *Ceram. Int.* **2021**, *47*, 29379−29385.
(36) Li, M.; Sun, P.; Song, Y.; Dai, G.; Zhang, J. Basic principles and research progress of laser simulation of ionization radiation effect in semiconductor devices. *J. Terahertz Sci. Electron. Inf. Technol.* **2015**, *13*, 160−168.
(37) Kim, D.-S.; Yoon, Y. J.; Lee, J. S.; Kang, I. M.; Lee, J. H. Experimental and simulation study of power performance improvement of GaN PIN betavoltaic cell. *Int. J. Energy Res.* **2021**, *45*, 17622−17630.
(38) Motaung, D. E.; Mhlongo, G. H.; Nkosi, S. S.; Malgas, G. F.; Mwakikunga, B. W.; Coetsee, E.; Swart, H. C.; Abdallah, H. M. I.; Moyo, T.; Ray, S. S. Shape-Selective Dependence of Room Temperature Ferromagnetism Induced by Hierarchical ZnO Nanostructures. *ACS Appl. Mater. Interfaces* **2014**, *6*, 8981−8995.
(39) Ding, S.; Chen, J. S.; Wang, Z.; Cheah, Y.; Madhavi, S.; Hu, X.; Lou, W. TiO_2 hollow spheres with large amount of exposed (001) facets for fastreversible lithium storage. *J. Mater. Chem.* **2011**, *21*, 1677.
(40) Shakil, M. R.; El-Sawy, A. M.; Tasnim, H.; Meguerdichian, A. G.; Jin, J.; Dubrosky, J. P.; Suib, S. L. Single-Doped and Multidoped Transition-Metal (Mn,Fe,Co,and Ni) ZnO and Their Electrocatalytic Activities for Oxygen Reduction Reaction. *Inorg. Chem.* **2018**, *57*, 9977−9987.
(41) Kannadasan, N.; Shanmugam, N.; Cholan, S.; Sathishkumar, K.; Viruthagiri, G.; Poonguzhali, R. The effect of Ce^{4+} incorporation on structural, morphological and photocatalytic characters of ZnO nanoparticles. *Mater. Charact.* **2014**, *97*, 37−46.
(42) Faisal, M.; Ismail, A. A.; Ibrahim, A. A.; Bouzid, H.; Al-Sayari, S. A. Highly Efficient Photocatalyst Based on Ce Doped ZnO Nanorods: Controllable Synthesis and Enhanced Photocatalytic Activity. *Chem. Eng. J.* **2013**, *229*, 225−233.
(43) Chang, C.; Lin, C.; Hsu, M. H. Enhanced photocatalytic activity of Ce-doped ZnO nanorods under UV and visible light. *J. Taiwan Inst. Chem. Eng.* **2014**, *45*, 1954−1963.
(44) Zheng, J. H.; Song, J. L.; Jiang, Q.; Lian, J. S. Enhanced UV Emission of Y-Doped ZnO Nanoparticles. *Appl. Surf. Sci.* **2012**, *258*, 6735−6738.
(45) Yang, J.; Wang, R.; Yang, L.; Lang, J.; Wei, M.; Gao, M.; Liu, X.; Cao, J.; Li, X.; Yang, N. Tunable Deep-Level Emission in ZnO Nanoparticles via Yttrium Doping. *J. Alloys Compd.* **2011**, *509*, 3606−3612.
(46) Hsu, C. L.; Wu, H. Y.; Fang, C. C.; Chang, S. P. Solution-Processed UV and Visible photodetectors based on Y-doped ZnO nanowires with TiO_2 nanosheets and Au nanoparticles. *ACS Appl. Energy Mater.* **2018**, *1*, 2087−2095.

https://doi.org/10.1021/acsomega.3c00039
ACS Omega 2023, 8, 17644−17652